JULY 01 2001

The prediction of façade effects from a point source above an impedance ground

Siu Hong Tang; Kai Ming Li

J. Acoust. Soc. Am. 110, 278–288 (2001)
https://doi.org/10.1121/1.1377049

The prediction of façade effects from a point source above an impedance ground

Siu Hong Tang and Kai Ming Li[a)]
Department of Mechanical Engineering, The Hong Kong Polytechnic University, Hong Kong

(Received 6 September 2000; accepted for publication 5 April 2001)

In many environmental noise prediction schemes, an empirical correction factor of 2.5 or 3.0 dB is normally added for the calculation of noise levels 1 meter in front of a reflecting façade. In this paper, theoretical and experimental studies have been conducted to examine the validity and accuracy of such approximations for a point source. The theoretical analysis involves the extension of the classical Weyl–van der Pol formula to include the effect of a reflecting façade. Experimental measurements have been conducted in an anechoic chamber to validate the theoretical predictions. It has been demonstrated that the simple empirical correction factor is adequate in cases for the assessment of the façade noise levels near the ground. However, this correction factor is not sufficient to predict the noise levels high above the ground. Some adjustments of the correction factor are required for a better estimation of sound fields in front of a reflecting façade above an impedance ground. © *2001 Acoustical Society of America.* [DOI: 10.1121/1.1377049]

PACS numbers: 43.50.Gf, 43.28.En, 43.50.Rq [MRS]

I. INTRODUCTION

The problem of noise is one of the most important environmental issues in recent years. With increased exposure and the greater sensitivity of much of the population, the number of noise-related complaints has grown at an alarming rate over the past few years. There is current legislation imposing limits of acceptable noise levels in many countries. However, in reflection of popular demand, these limits look set to be tightened further in the future. There has been an increased interest in the development of accurate numerical schemes for the prediction of environmental noise in a complex urban environment.[1–3]

A typical situation that requires the prediction of noise levels is for buildings situated close to a road of high traffic volume. As a general rule of thumb, a correction factor of 3 dB (or 2.5 dB for the guideline developed in the UK[4]) has been widely used for the calculation of noise in front of a reflecting façade. This empirical correction factor is related to sound propagation from an incoherent line source radiating noise from a continuous traffic flow. More recently,[5] a sequence of point sources has been used to model the traffic flow on a road in which each vehicle is treated as an equivalent point source. The total sound field is obtained by summing contributions from these point sources incoherently. However, many outdoor ground surfaces have different acoustical characteristics ranging from hard reflecting ground to grassland of fairly high flow resistivity and snow-covered ground of low flow resistivity.[6] It is well-known that the effect of ground impedance has greatly influenced the overall sound-pressure level received at a modest distance from the noise source. Therefore, an addition of a single empirical correction factor in front of the façade due to this reflection of sound may not be adequate to represent the whole situation.

In a series of studies,[7] we wish to investigate the interference effects of a point source and its images in a complex urban environment. In the present study, we examine a somewhat less complicated urban situation: the façade effect on the propagation of sound due to a point source above an impedance ground. Theoretical and experimental studies will be conducted to investigate the effect of the reflecting plane on the spectrum received at some distance away from the noise source. Although meteorological and topographical conditions have significant effects on sound propagation outdoors, they are ignored in the present study because our principal aim is to explore the effect of a reflecting façade above an absorbing ground.

Theoretical prediction of sound fields near a reflecting wall involves an extension of the classical Weyl–van der Pol theory to include the effect of a reflecting façade. The theory behind the prediction model is outlined in Sec. II. Indoor experiments are conducted to validate the theoretical model and they are presented in Sec. III. In Sec. IV, we use the theoretical model to calculate the sound fields above three different types of ground surfaces in front of a reflecting façade. Finally, some concluding remarks are offered in Sec. V.

II. THEORY

There is extensive literature for the sound field above an absorbing ground.[8–10] However, the asymptotic solution for a harmonic source above an absorbing ground in the presence of a reflecting façade is not readily available in the literature. Hence, it is derived and included here for future reference, although many authors would have written down the solution empirically without going through detailed asymptotic evaluation. The basic formulation for the sound field above an impedance ground in vicinity of a façade is as follows. Without loss of generality, the impedance ground is

[a)]Author to whom correspondence should be addressed. Electronic mail: mmkmli@polyu.edu.hk

located at the plane of $z=0$, the reflecting façade located at the plane of $x=0$, and a harmonic source located at $(x_s,0,z_s)$ where $x_s, z_s>0$. We wish to determine the sound field for the quarter in which $x>0$ and $z>0$; see Fig. 1 for the schematic diagram of the problem. The time-dependent factor, $e^{-i\omega t}$, is understood and suppressed for brevity in our subsequent analysis. The propagation of sound, as represented by the velocity potential, is governed by the inhomogeneous Helmholtz equation

$$\nabla^2\phi+k^2\phi=-\delta(x-x_s)\,\delta(y)\,\delta(z-z_s), \tag{1}$$

where k is the wave number given by ω/c with ω the angular frequency of the source and c the speed of sound in air. Specifying the plane of $z=0$ to be an absorbing ground of effective admittance β_z and the plane of $x=0$ to be a reflecting façade of effective admittance β_x, the velocity potential must satisfy the boundary conditions

$$\frac{\partial\phi}{\partial z}+ik\beta_z\phi=0 \quad \text{at} \quad z=0, \tag{2}$$

and

$$\frac{\partial\phi}{\partial x}+ik\beta_x\phi=0 \quad \text{at} \quad x=0. \tag{3}$$

There is an inherent assumption of the above boundary conditions: the angle between the flat ground and façade is $\pi/2$, i.e., the two surfaces are perpendicular to each other. This assumption is not too restrictive and is generally applicable for the case where the prediction of sound fields exterior to a tall building is required.

The posed problem can be solved readily by representing the solution in terms of Fourier integrals as follows. According to the theory of geometrical acoustics (see, for example, Ref. 11, Sec. 9.8), the source and its three images can be identified immediately as shown in Fig. 1, but careful considerations are necessary. We have to take into account the diffracted waves as a result of reflections from the impedance ground and façade. The positions of all ''sources'' can be identified straightforwardly as $(x_s,0,z_s)$, $(x_s,0,-z_s)$, $(-x_s,0,z_s)$, and $(-x_s,0,-z_s)$. We also note that according to the geometrical-acoustic principles,[11] there will be no wave diffraction term due to the inside edge of the wedge because its angle is $\pi/2$. Also, we ignore the diffraction wave contribution due to the impedance discontinuity (i.e., the ground and façade have different impedance) at the edge. These two assumptions can be supported by the good agreement of the theoretical prediction and experimental results for the case of ground and/or façade having different impedance; see Sec. III below.

Assuming the sound field is composed of four terms due to the source and its images, we can write the solution in the form of

$$\begin{aligned}
\phi=&-\frac{1}{(2\pi)^3}\int_{-\infty}^{\infty}\int_{-\infty}^{\infty}\int_{-\infty}^{\infty}\frac{\exp[ik_x|x-x_s|+ik_y y+ik_z|z-z_s|]}{k^2-k_x^2-k_y^2-k_z^2}\,dk_x\,dk_y\,dk_z\\
&-\frac{1}{(2\pi)^3}\int_{-\infty}^{\infty}\int_{-\infty}^{\infty}\int_{-\infty}^{\infty}V_z\,\frac{\exp[ik_x|x-x_s|+ik_y y+ik_z(z-z_s)]}{k^2-k_x^2-k_y^2-k_z^2}\,dk_x\,dk_y\,dk_z\\
&-\frac{1}{(2\pi)^3}\int_{-\infty}^{\infty}\int_{-\infty}^{\infty}\int_{-\infty}^{\infty}V_x\,\frac{\exp[ik_x(x-x_s)+ik_y y+ik_z|z-z_s|]}{k^2-k_x^2-k_y^2-k_z^2}\,dk_x\,dk_y\,dk_z\\
&-\frac{1}{(2\pi)^3}\int_{-\infty}^{\infty}\int_{-\infty}^{\infty}\int_{-\infty}^{\infty}V_{xz}\,\frac{\exp[ik_x(x+x_s)+ik_y y+ik_z(z+z_s)]}{k^2-k_x^2-k_y^2-k_z^2}\,dk_x\,dk_y\,dk_z,
\end{aligned} \tag{4}$$

where V_z, V_x, and V_{xz} are the plane-wave reflection coefficients due to the reflections from the impedance ground and façade. They can be determined by applying the boundary conditions, Eqs. (2) and (3), on Eq. (4). With some tedious algebraic manipulations, we can show that

$$V_z=\frac{k_z-k_0\beta_z}{k_z+k_0\beta_z}, \tag{5a}$$

$$V_x=\frac{k_x-k_0\beta_x}{k_x+k_0\beta_x}, \tag{5b}$$

and

$$V_{xz}=V_x\times V_z=\frac{k_x-k_0\beta_x}{k_x+k_0\beta_x}\times\frac{k_z-k_0\beta_z}{k_z+k_0\beta_z}. \tag{5c}$$

Note also that negative signs are present in all integrals in Eq. (4) as a result of the specification of the problem where a source of strength -1 is used in Eq. (1).

In Eq. (4), we can identify that the first term corresponds to the direct wave term. The second and third terms correspond to waves, which have a single reflection from the impedance ground and the façade, respectively. The last term of Eq. (4) corresponds to the wave emanating from the source that hits the ground and façade before reaching the receiver. Although it is possible to evaluate these integrals numerically by means of the standard Gauss–Laguerre technique, as detailed in Ref. 9, we prefer to use the technique of contour integration for the derivation of a closed-form analytical formula which results in a better understanding of the problem. It is because the analytical approach invariably leads to a

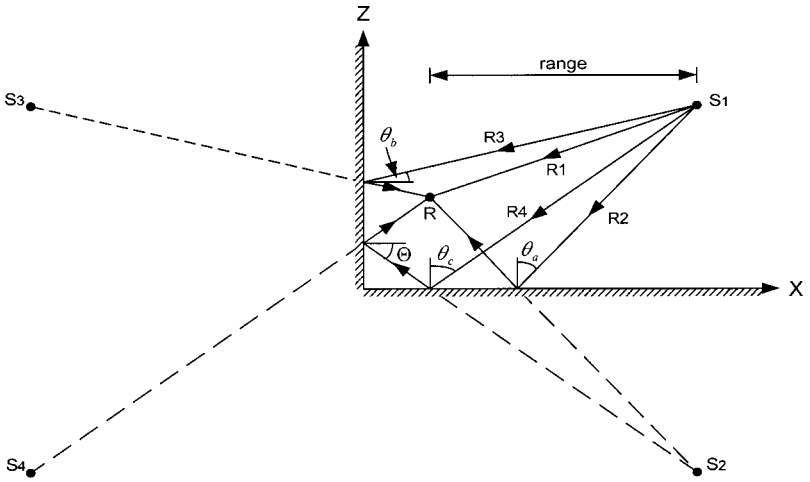

FIG. 1. The source/receiver geometry: three image sources and the sound paths due to the direct wave are shown.

physically interpretable solution in which contributions due to the reflected waves from each of the three image sources can be identified immediately.

Each of the Fourier integrals in Eq. (4) can be estimated asymptotically and their details are relegated to the Appendix. As expected, the solution can be cast in a form of the classical Weyl–van der Pol formula

$$\phi = \frac{e^{ikR_1}}{4\pi R_1} + Q(R_2,\theta_a,\beta_z)\frac{e^{ikR_2}}{4\pi R_2} + Q(R_3,\theta_b,\beta_x)\frac{e^{ikR_3}}{4\pi R_3} + Q(R_4,\theta_c,\beta_z)Q(R_4,\Theta,\beta_x)\frac{e^{ikR_4}}{4\pi R_4}, \tag{6}$$

where Q is the corresponding spherical wave reflection coefficient for the wave reflected from the ground and the façade. The path lengths R_1, R_2, R_3, and R_4 are the distances from the source and its three images to the receiver, respectively. The variables θ_a, θ_b, and θ_c are angles of incidence of reflected waves measured from the normal to the reflecting plane; see Fig. 1. Also, θ_c and Θ are related according to $\cos\Theta = \cos\psi \sin\theta_c$, where ψ is the azimuthal angle of the vertical plane that contains both source and receiver.

Knowing the distance between the image source and receiver (R), the angle of incidence of the reflected wave (θ), and the specific admittance of the reflecting surface (β), the spherical wave reflection coefficient can be determined according to

$$Q(R,\theta,\beta) = R_p + (1-R_p)F(w), \tag{7}$$

where

$$R_p = \frac{\cos\theta - \beta}{\cos\theta + \beta}, \tag{8}$$

$$F(w) = 1 + i\sqrt{\pi} w e^{-w^2}\,\mathrm{erfc}(-iw), \tag{9}$$

and

$$w = +\sqrt{\tfrac{1}{2}ikR}(\cos\theta + \beta). \tag{10}$$

We can see from Eq. (6) that there are two extra terms in the Weyl–van der Pol formula as a result of the presence of reflecting façade above an impedance ground. In fact, the surface wave term is present implicitly in the boundary loss factor $F(w)$, cf. Eq. (9).[12] Hence, all surface wave components are inherently included in the derived formula, Eq. (6). The validity of the derived formula will be confirmed by comparing with experimental measurements indoors.

We also wish to point out that there are many other more accurate asymptotic formulations (see, for example Refs. 13 and 14), and other computationally intensive numerical methodologies (see, for example, Ref. 15) for the computation of the sound fields above an impedance ground. On the other hand, a set of relatively stringent requirements ($kR \gg 1$, $|\beta_e| \ll 1$, and $\theta \approx \pi/2$) is used in deriving the spherical reflection coefficient.[8] However, numerical comparisons of various computational schemes do not reveal any significant discrepancies from that predicted by the Weyl–van der Pol formula for practical geometries and typical outdoor surfaces.[16–18] As the Weyl–van der Pol formula is now widely accepted for predicting outdoor sound,[10,12] we shall use it and its analogous form in our following analysis.

III. EXPERIMENTAL VALIDATIONS

The investigation of the predicted sound field near a building façade involves a simple mathematical modeling as shown in Sec. II. To validate the theoretical model, experiments are conducted in an anechoic chamber of size 6×6×4-m (high). The experimental model is composed of two 2.4×1.8×0.02-m (thick) hardwood boards making contact at one of their edges so that they are aligned at a right angle with each other. The sound field within the region in front of the vertical board consists of a main noise source and three images. The hardwood boards were varnished to provide smooth hard surfaces for parts of the experiments. Two different types of materials, a 1-cm-thick carpet and 4-cm-thick fiberglass, were also used to cover the hardwood board, providing surfaces of finite effective impedance. A combination of the ground and façade with different covering materials was used for measurements.

For the carpet-covered surface, it can be modeled as a locally reacting ground where a two-parameter model[19] can be used to predict the effective admittance as follows:

$$\beta_e = \frac{1}{0.436(1+i)(\sigma_e/f)^{0.5} + 19.48 i\alpha_e/f}. \tag{11}$$

In the above equation, σ_e is the effective flow resistivity and α_e is the effective rate of change of porosity with depth of the material. On the other hand, an extended reaction model should be used to estimate the impedance of the surface covered with a layer of fiberglass. For the fiberglass used in our experiments, we find that a one-parameter Delaney and Bazley model[20] can be used conveniently to calculate the effective admittance of the fiberglass-covered ground. The real and imaginary parts of the normalized impedance of the ground ($Z_1 = Z_R + iZ_X$), which are dependent on the flow resistivity of ground, are determined by

$$Z_R = 1 + 9.08(\sigma_e/f)^{0.75}, \tag{12}$$

$$Z_X = 11.9(\sigma_e/f)^{0.73}. \tag{13}$$

For the extended reaction ground, the effective admittance β_e is determined by[21]

$$\beta_e = m\sqrt{n^2 - \sin^2\theta}, \tag{14}$$

where $m(\equiv k_1/k = c/c_1)$ is the sound-speed ratio n $(\equiv \rho/\rho_1)$ is the density ratio. In these two ratios, ρ is the density of air and the subscript 1 denotes the corresponding properties of the ground. The real and imaginary parts of the wave number of the ground $k_1(k_1 = k_R + ik_x)$ are given by

$$k_R/k = 1 + 10.8(\sigma_e/f)^{0.70}, \tag{15}$$

$$k_X/k = 10.3(\sigma_e/f)^{0.59}. \tag{16}$$

Use of Eqs. (12)–(16) and the relationship of $1/Z = mn$ permit the determination of the effective admittance of the fiberglass-covered ground. In their paper, Li *et al.*[21] have demonstrated that use of Eq. (14) in the Weyl–van der Pol formula leads to accurate predictions of sound fields even for materials with flow resistivity as low as 1000 Pa s m^{-2}. Since the outdoor ground surfaces normally have much higher flow resistivity, we shall use this ''effective admittance approach'' in our subsequent numerical simulations.

A Tannoy driver with a tube of 3 cm internal diameter and 1 m long was used as a point source in all indoor experiments. The sound source was connected to a maximum length sequence system analyzer (MLSSA) with an MLS card installed in a PC.[22] The analyzer was connected to a B&K 2713 amplifier. The MLSSA system was used both as the signal generator for the source and as the signal-processing analyzer. A BSWA TECH MK224 $\frac{1}{2}$-in. condenser microphone and a BSWA TECH MA201 preamplifier were used together as the receiver. Both source and receiver were placed at a fixed position by means of a stand; clamps and the position of receiver were adjusted for different sets of measurements.

To characterize the acoustical properties of the indoor ground surfaces, prior measurements were conducted with the carpet and fiberglass, in turn, secured on the hardwood board. Theoretical predictions were compared with experimental measurements for the propagation of sound over an impedance ground, enabling the determination of the ground parameters. A graphical representation of the setup for the ground characterization is shown in Fig. 2. Measurements above the carpet and fiberglass for different source and receiver geometry were obtained. These measurements were

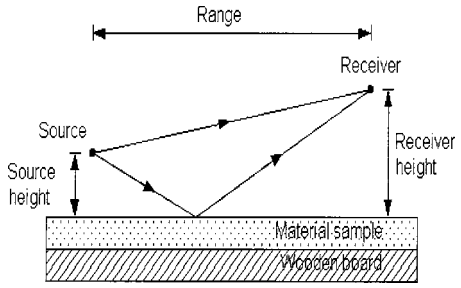

FIG. 2. The source/receiver geometry: characterization of the indoor ground surfaces.

subsequently fitted by means of a two-parameter model;[19] [see Eq. (12)], for the carpet and by means of a one-parameter model[20] for the fiberglass. Best-fit parameters were found to be $\sigma_e = 10\,000$ Pa s m^{-2} and $\alpha_e = 80$ m^{-1} for the carpet and an effective flow resistivity of 35 000 Pa s m^{-2} for fiberglass. Figures 3 and 4 display typical experimental measurements and theoretical predictions of the relative sound-pressure level with the reference free-field level measured at 1 m. These ground parameters and measurement geometries have been used in our subsequent prediction of the propagation of sound above an impedance ground in the presence of a reflecting façade.

To validate the theoretical model developed in Sec. II, three sets of indoor experiments were conducted in which the spectra of relative sound-pressure levels were obtained with different horizontal ranges between the source and receiver. Due to the physical limitations of the anechoic chamber, the range is chosen to vary from 0.6 to 1.5 m at 0.1-m intervals for each measurement. It is worth pointing out that the principal aim of our indoor measurements is to provide useful experimental data for the validation of Eq. (6). They are not intended to be proper scale model experiments, as conducted by others.[23] Hence, we made no attempt to select the most appropriate materials to model the porous ground and absorbing façade. Rather, we chose a hardwood board to model

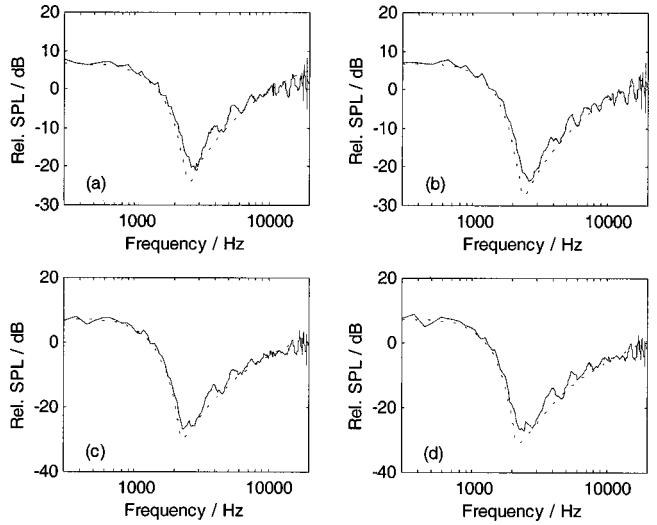

FIG. 3. Characterization of a hard ground covered with carpet. Source height = 0.05 m, receiver height = 0.04 m. Range: (a) 0.6 m; (b) 0.8 m; (c) 1.0 m; (d) 1.2 m. (Dotted line: theoretical prediction; Solid line: experimental result.)

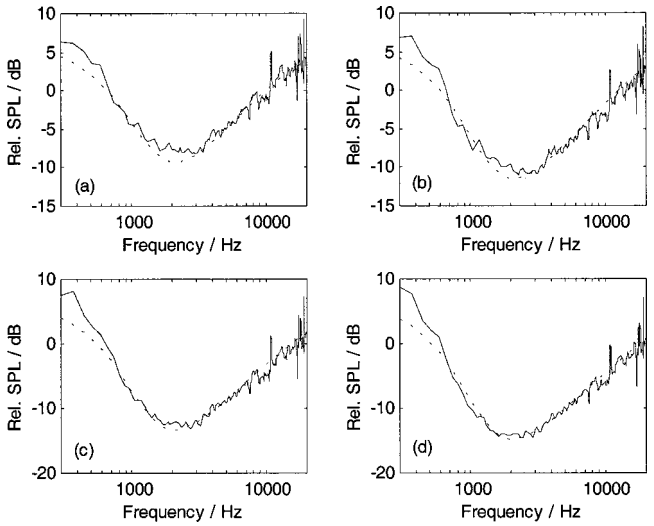

FIG. 4. Characterization of a hard ground covered with fiberglass. Source height = 0.05 m, receiver height = 0.04 m. Range: (a) 0.6 m; (b) 0.8 m; (c) 1.0 m; (d) 1.2 m. (Dotted line: theoretical prediction; Solid line: experimental result.)

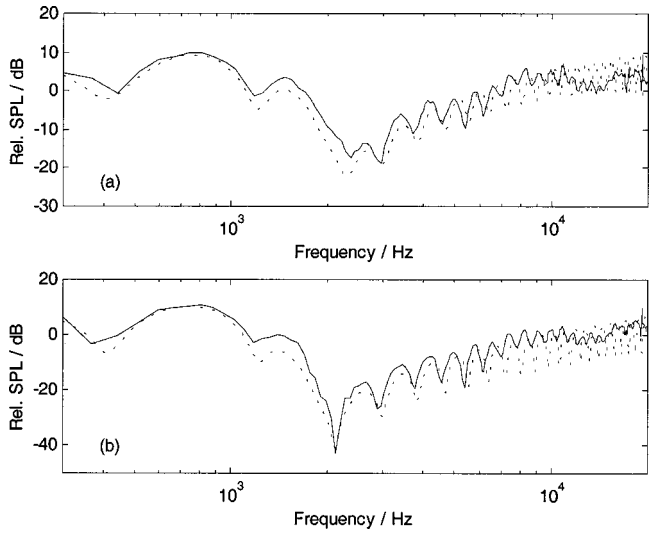

FIG. 6. Experimental data and theoretical predictions for sound propagation over a carpet-covered floor and a hard vertical wall. Source height=0.06 m, receiver height=0.05 m at 0.2 m from façade. Range: (a) 0.6 m; (b) 1.4 m. (Dotted line: theoretical prediction; Solid line: experimental result.)

a hard ground, a carpet-laid surface to model a locally reacting ground, and a surface covered with fiberglass to model an extended reaction ground. But, nevertheless, comparisons of the indoor experimental results and theoretical predictions should shed light on the validity of Eq. (6) in modeling the façade effects numerically.

In the first experimental measurements, hardwood boards were used as the floor and the vertical wall. In this case, both β_z and β_x vanish, and hence, all spherical wave reflection coefficients equal to 1. Equation (6) is used to compute the sound fields that are used to compare with the experimental measurements. Figure 5 shows measured and predicted sound fields as a function of frequency. The receiver was placed 5 cm above the floor and 20 cm in front of the vertical wall. The source was located 6 cm above the floor and at the same principal plane as the receiver, which is mutually perpendicular to the ground and façade. The theoretical predictions are in accord with the experimental measurements. As expected, in the presence of a reflecting façade, the interference patterns in the frequency spectrum are much more intricate as a result of the existence of two extra terms in the Weyl–van der Pol formula.

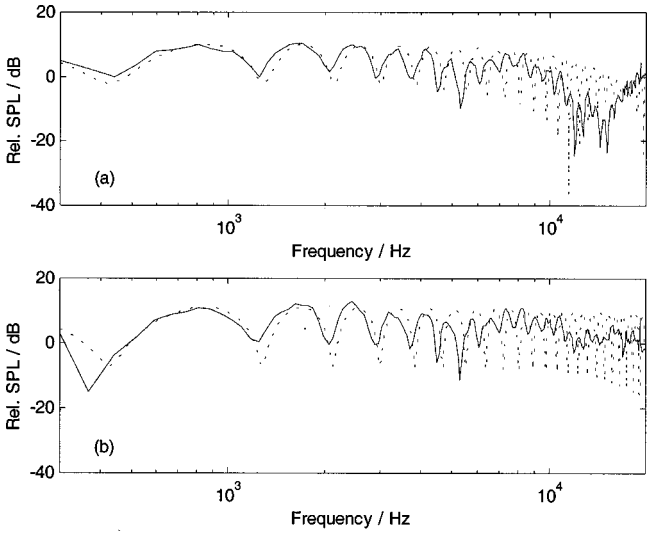

FIG. 5. Experimental data and theoretical predictions for sound propagation over a hard floor in front of a hard vertical wall. Source height=0.06 m, receiver height=0.05 m at 0.2 m from façade. Range: (a) 0.6 m; (b) 1.4 m. (Dotted line: theoretical prediction; Solid line: experimental result.)

In the second set of measurements, the carpet was secured on the surface of the horizontal board and the other hardwood board was used as the vertical wall. The orientation of the source and receiver was the same as in the first set of measurements. The source and receiver heights were now measured from the surface of the carpet instead of the floor. Figure 6 displays typical sets of measured data. Good agreement is obtained with the theoretical predictions according to Eq. (6).

In the last case, a layer of 4-cm-thick fiberglass was attached to the surface of the vertical wall, with no change of the source and receiver orientation. The experimental results for the last set of measurements are shown in Fig. 7. Again, the agreement between theoretical predictions and experimental data is generally good. We note that although there are considerable differences in the magnitude of the relative sound-pressure levels, especially at high frequencies in Fig. 5, the positions of interference ''dips'' can be predicted closely by the theoretical model. The discrepancies in the magnitude could be attributed to the fact that the wooden board (vertical wall and ground surfaces) has a nonzero effective acoustic admittance.

IV. PREDICTION OF FAÇADE EFFECTS IN THE PRESENCE OF AN IMPEDANCE GROUND

In Sec. III, we have presented experimental results for the sound fields above an impedance ground in front of a vertical wall. These experimental results agree reasonably well with the theoretical model developed in Sec. II. This gives us the confidence of using the theory to simulate a slightly more complex outdoor environment when the re-

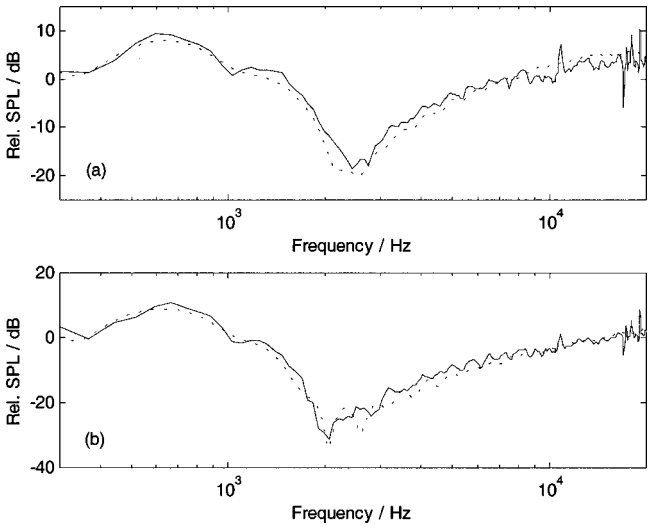

FIG. 7. Experimental data and theoretical predictions for sound propagation over a carpet-covered floor and a hard vertical wall covered with fiberglass. Source height=0.06 m, receiver height = 0.05 m at 0.2 m from façade. Range: (a) 0.6 m; (b) 1.4 m. (Dotted line: theoretical prediction; Solid line: experimental result.)

ceiver is situated above an impedance ground, and is in close proximity to a building façade. As a general rule in many environmental noise prediction schemes, a correction factor of 3 dB (2.5 dB for the guideline developed in the UK[4]) is added to account for the façade effect, as the vertical wall is assumed to be an acoustically hard surface. Here, we shall investigate the validity of such approximation as follows.

In the present study, the distribution of an A-weighted sound-pressure level (SPL) in front of a building façade is simulated. Two types of sources, noise from tire–road interactions and from engines, are taken into consideration because they represent typical sources in the context of environmental noise. The source heights used in the analysis for tire and engine exhaust are 0.01 and 0.3 m, respectively. Although it is possible for us to study the case in which the vertical wall has finite impedance, we assume that it has a perfectly reflecting surface because a building façade is normally a fairly hard surface with materials of high flow resistivity. Three different ground surfaces outside a building are considered. The first one is a typical hard ground, such as a concrete road surface, with negligible effective admittance. The second case to be considered is a simulation of grassland. The two-parameter model with $\sigma_e = 250$ kPa s m^{-2} and $\alpha_e = 100$ m^{-1} is used to calculate the impedance of the grassland. The last case is a snow-covered ground where a simple one-parameter hard-back layer model[21] is used with $\sigma_e = 20$ kPa s m^{-2} and the snow depth of 0.1 m.

In all calculations (i) both source and receiver are situated at the ''principal'' plane which is mutually perpendicular to the ground and façade, and (ii) the receiver is located 1 m in front of the façade. For the ease of interpretation, the numerical simulation is plotted for the difference between the A-weighted sound-pressure level with ($\mathrm{SPL_W}$) and without ($\mathrm{SPL_{W/O}}$) the presence of the reflecting façade

$$\Delta(z) = \mathrm{SPL_W} - \mathrm{SPL_{W/O}}.$$

The case being investigated involves the noise source situated up to 20 m from the reflecting façade and the receiver placed up to 20 m from the ground. Figures 8(a)–(c) show contour plots of the distribution $\Delta(z)$ with the source located 0.01 m above three different types of ground.

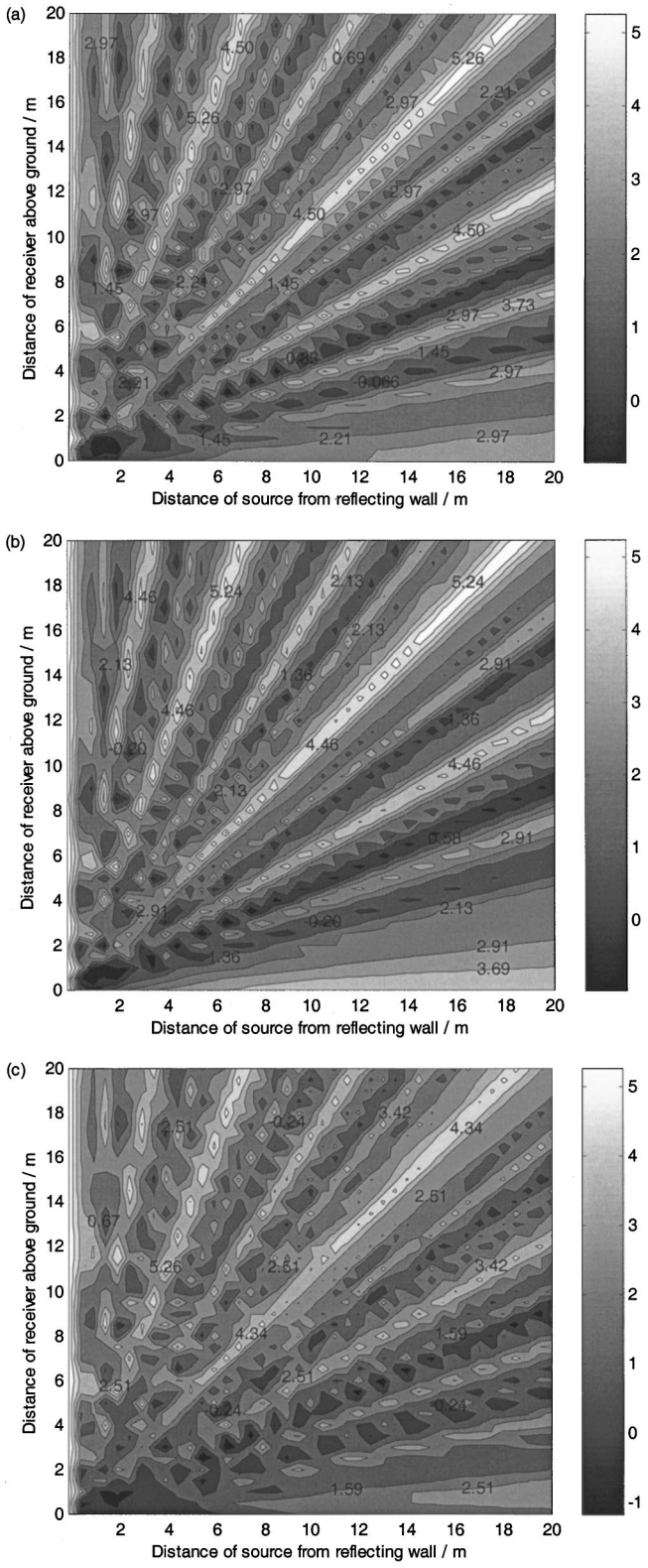

FIG. 8. Predicted difference in A-weighted sound-pressure levels with and without a reflecting façade for tire noise located at 0.01 m above the ground. (a) Hard ground, hard façade; (b) grassland, hard façade; (c) snow-covered ground, hard façade.

TABLE I. Mean values and standard deviations of A-weighted sound-pressure level difference of tire noise.

Distance from façade (m)	Hard ground Mean (dB)	Hard ground Standard deviation (dB)	Grassland Mean (dB)	Grassland Standard deviation (dB)	Snow-covered ground Mean (dB)	Snow-covered ground Standard deviation (dB)
4	2.06	1.32	2.04	1.30	2.07	1.26
8	2.23	1.25	2.19	1.27	2.05	1.15
12	2.37	1.34	2.39	1.36	2.14	1.34
16	2.47	1.30	2.51	1.35	2.24	1.23
20	2.29	1.15	2.30	1.20	1.98	1.07

In these predictions, the source has a broadband spectrum of equal energy in all octave bands, i.e., a white-noise source. The abscissa and ordinate of Fig. 8 represent, respectively, the horizontal distance of the source from the façade and the vertical distance of the receiver from the ground. In the contour plots, those regions that show a level of 3.0 dB (or 2.5 dB for the British guideline) are considered to be satisfactory in applying the empirical factor to correct for the façade effect. Predictions at other planes are not shown as they have a rather similar trend to those shown in the principal plane.

A close examination of Fig. 8 reveals that the façade correction of 2.5 or 3 dB is generally acceptable if the source is near the ground. However, the spread of Δ (i.e., the difference between the maximum and minimum values) for all three impedance grounds is about 6 dB. To allow for the assessment of a simple façade correction at all heights, it is useful to consider the mean value of Δ where the receiver is located at a given distance from the façade. The mean value, Δ, and its standard deviation, s.d., can be determined by

$$\bar{\Delta}=\frac{\int_0^{h_{\max}}\Delta(z)dz}{h_{\max}} \quad \text{and} \quad \text{s.d.}=\frac{\int_0^{h_{\max}}\Delta^2(z)dz}{h_{\max}},$$

where $h_{\max}$ is the maximum height of the receiver used in this statistical analysis. They can be computed easily by a simple numerical integration method.

Table I shows the mean values and the corresponding standard deviations of Δ for the case of tire noise with $h_{\max}$ of 20 m. The mean values and the corresponding standard deviations are close for the case of hard ground and grassland. The snow-covered ground has slightly different values from the other two grounds. This indicates that different impedance grounds do not have significant contributions towards the change in Δ because the source is very near to the ground. In general, Δ is close to the empirical correction factor of 2.5 dB. The confidence level of the predicted SPL difference in front of the façade for different source locations would be expected to fall mainly within the first deviation from the mean values (i.e., mean$\pm$standard deviation). Therefore, it may seem reasonable to assume that the addition of the empirical correction factor is an acceptable guideline in this case. However, it may not be suitable in applying this guideline for an elevated source as we investigate the case for an engine noise source located 0.3 m above the impedance ground.

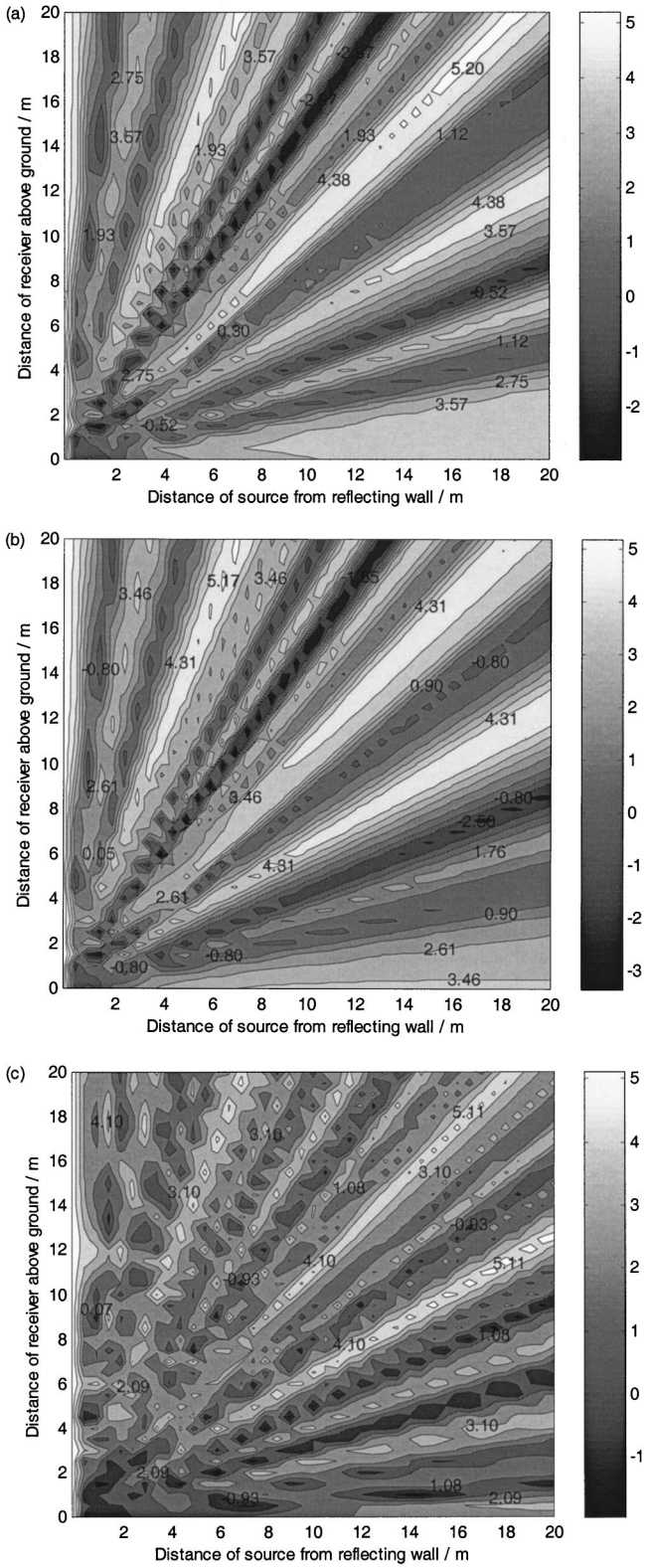

FIG. 9. Predicted difference in A-weighted sound-pressure levels with and without a reflecting façade for engine noise located at 0.3 m above the ground. (a) Hard ground, hard façade; (b) grassland, hard façade; (c) snow-covered ground, hard façade.

Similar contour plots are shown in Figs. 9(a)–(c) for the source located 0.3 m above the ground of different impedance. In this example, a measured noise spectrum for automobiles operating at 30 mph is used[24] instead of the white-

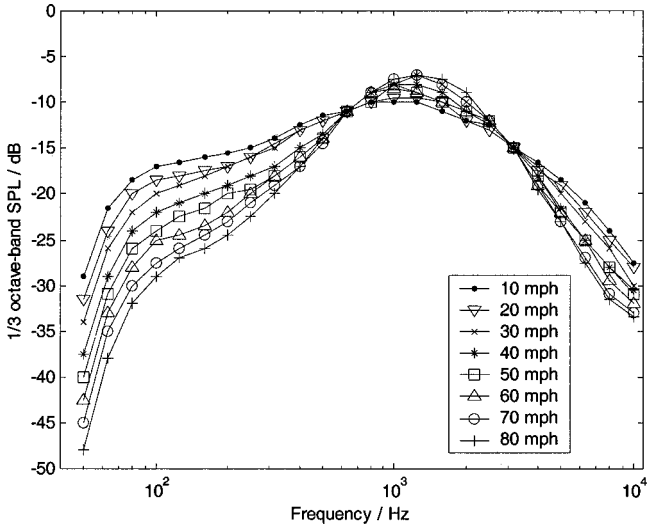

FIG. 10. Emission spectra for automobiles of different speed on average pavement one-third-octave band spectra, relative to A-weighted sound-level emissions.

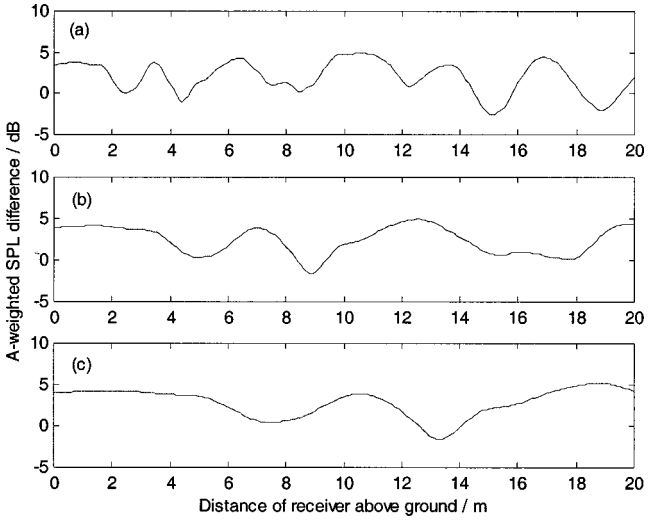

FIG. 11. The predicted A-weighted SPL difference along the height of a building when noise source (engine) is located above a hard ground at (a) 10 m; (b) 20 m; and (c) 30 m from the reflecting façade.

noise spectrum used in the case of tire noise. Figure 10 displays the noise spectra for automobiles operating at different speeds from 10 to 80 mph. It shows that their main differences are at the low frequency contents (below 300 Hz), which are less important in the A-weighted assessment. Hence, we expect that the theoretical predictions for the automobile operating at other speeds do not change significantly and, therefore, for brevity they will not be shown here.

For the contour plots of engine noise, the variation trends in Δ are rather similar to that of the tire noise contour plots. However, the spread of Δ is 7- and 8-dB for snow-covered and hard ground, respectively, and a slightly larger spread of about 8.5 dB is found for grassland. Table II shows the mean values and the corresponding standard deviations of Δ for the case of engine noise.

The standard deviation tends to increase slightly before it drops down with respect to the distance of source away from the reflecting wall. This is because when the source is about 10 m away from the façade, more changes in sound levels are detected in the prediction. Therefore, a higher degree of fluctuation of sound will be experienced. Also, it would be expected that the standard deviation decreases gradually as the source is moved further away from the façade since less fluctuation of sound level is predicted. Figures 11(a)–(c) show the relationship, with engine noise over a hard ground, between the predicted SPL difference in front of the façade due to the variation of source distance at 10, 20, and 30 m from the façade surface. When the noise source is near to a façade (in this case 10 m), a receiver in front of the wall will experience a very random change in sound level as it goes up from the ground. However, if the source moves further away from the façade to distances such as 20 or 30 m, the change in sound level that it experiences will become less random. Therefore, one would expect that at distances even further away from the façade, the SPL difference with respect to the variation of height is to be fairly stable. The phenomenon is similar for both tire and engine exhaust noise above different impedance surfaces.

In the case of grassland, the standard deviations are slightly higher than that of the hard and snow-covered ground, hence leading to a larger range of sound-level difference for grassland observed earlier.

Better agreement with the correction factor is found in the region near the ground for both cases of noise source. This agreement is enhanced if the source is located further away from the façade. In general, the agreement works well up to 4 m above the ground if the source is located 20 m away from the façade. However, the accuracy is in doubt for the SPL difference values higher up the ground because of a rather large amount of fluctuation. For engine exhaust noise, a maximum of about 3-dB addition and a minimum of about 6-dB reduction relative to the correction factor are found in some regions in front of the façade as the source is moved away from it. A slightly lower reduction of about 4 dB is found for the case of tire noise. Therefore, the addition of a correction factor may not seem to be totally effective in regions high above the ground and some adjustments may be required.

TABLE II. Mean values and standard deviations of A-weighted sound-pressure level difference of engine noise.

	Hard ground		Grassland		Snow-covered ground	
Distance from façade (m)	Mean (dB)	Standard deviation (dB)	Mean (dB)	Standard deviation (dB)	Mean (dB)	Standard deviation (dB)
4	2.12	1.65	1.96	1.73	1.87	1.37
8	2.23	1.82	1.98	1.84	2.13	1.47
12	2.30	1.87	1.93	1.95	2.12	1.42
16	2.61	1.71	2.13	1.88	2.23	1.51
20	2.42	1.67	1.85	1.75	2.06	1.45

V. CONCLUDING REMARKS

The asymptotic formula has been derived for the sound field due to a point source above a ground surface in front of a reflecting façade. The formula is validated by comparison

with precise indoor measurements conducted in an anechoic chamber. As expected, the analytical solution is composed of four terms (a source and three image sources) as a result of the reflections from the absorbing ground and façade.

We also examine the guideline of using an additional empirical correction factor of 2.5 or 3.0 dB at 1 m in front of a reflecting façade in many noise prediction schemes. It has been found that an addition of the correction factor for the A-weighted SPL is generally acceptable when the point source is close to the ground. However, the prediction is less satisfactory for an evaluated source above a ground of finite impedance. Some modifications and a stricter condition of using the empirical correction factor are required if a more accurate prediction is needed.

ACKNOWLEDGMENTS

This research was supported in part by the Research Grants Council of the Hong Kong Special Administrative Region (Project No.: PolyU 5151/99E) and the Hong Kong Polytechnic University. S.H.T. gratefully acknowledges the financial support of the Research Committee of the Hong Kong Polytechnic University for the Research Studentship.

APPENDIX: ASYMPTOTIC EVALUATION OF FOURIER INTEGRALS

Let the four separate integrals in Eq. (4) be I_1, I_2, I_3, and I_4. Using the method of contour integration (see for example, Ref. 25), the outer integral of I_1 with respect to k_z can be evaluated exactly to give

$$I_1=\frac{-i}{(2\pi)^2}\int_{-\infty}^{\infty}\int_{-\infty}^{\infty}\frac{\exp\{ik_x|x-x_s|+ik_y y+ik_z^*|z-z_s|\}}{2k_z^*}\times dk_x\,dk_y, \tag{A1}$$

where

$$k_z^*=\sqrt{k^2-k_x^2-k_y^2}. \tag{A2}$$

The root taken for k_z^* should be positive real and negative imaginary such that finite amplitude in I_1 can be ensured. We can identify Eq. (A1) as the Sommerfeld integral,[26] which can be evaluated exactly to give

$$I_1=\frac{\exp(ikR_1)}{4\pi R_1}. \tag{A3}$$

We can see that I_1 may be regarded as the direct wave term where R_1 is the distance from the source to receiver; see Fig. 1 for the source–receiver configuration. Alternatively, we can evaluate the k_x integral by the method of contour integration to give

$$I_1=\frac{-i}{(2\pi)^2}\int_{-\infty}^{\infty}\int_{-\infty}^{\infty}\frac{\exp\{ik_x^*|x-x_s|+ik_y y+ik_z|z-z_s|\}}{2k_x^*}\times dk_y\,dk_z, \tag{A4}$$

where

$$k_x^*=\sqrt{k^2-k_y^2-k_z^2}, \tag{A5}$$

and, again, the root for k_x^* is taken to be positive real and negative imaginary. The integral in Eq. (A4) is the Sommerfeld integral and its solution is given in Eq. (A3) as expected.

We can apply the same method in the integrals, I_2 and I_3 with the evaluation of k_z integral first for I_2 and k_x integral first for I_3. The reason for the choice of the order in the integration is obvious because of the presence of an extra term, V_z and V_x, in I_2 and I_3 respectively. We can simplify the integrals as follows:

$$I_2=\frac{-i}{(2\pi)^2}\int_{-\infty}^{\infty}\int_{-\infty}^{\infty}\frac{k_z^*-k_0\beta_z}{k_z^*+k_0\beta_z}\times\frac{\exp\{ik_x|x-x_s|+ik_y y+ik_z^*(z+z_s)\}}{2k_z^*}dk_x\,dk_y, \tag{A6}$$

and

$$I_3=\frac{-i}{(2\pi)^2}\int_{-\infty}^{\infty}\int_{-\infty}^{\infty}\frac{k_x^*-k_0\beta_x}{k_x^*+k_0\beta_x}\times\frac{\exp\{ik_x^*(x+x_s)+ik_y y+ik_z|z-z_s|\}}{2k_x^*}dk_y\,dk_z. \tag{A7}$$

Using the standard method of steepest descents with the aid of the pole subtraction method,[27] we can evaluate I_2 and I_3 straightforwardly to give the asymptotic solutions as

$$I_2=Q(R_2,\theta_a,\beta_z)\frac{e^{ikR_2}}{4\pi R_2}, \tag{A8}$$

and

$$I_3=Q(R_3,\theta_b,\beta_x)\frac{e^{ikR_3}}{4\pi R_3}. \tag{A9}$$

Finally, I_4 can be estimated asymptotically in an analogous manner, but there is a slight complication as the integrand contains the reflection factors, V_x and V_z. There are two interesting cases for consideration in the context of the façade effect on sound propagation outdoors. The first case is when the angle of incidence θ_c (see Fig. 1 for the nomenclature) is close to $\pi/2$. In this case, we can evaluate the k_z integral first to yield

$$I_4=\frac{-i}{(2\pi)^2}\int_{-\infty}^{\infty}\int_{-\infty}^{\infty}\frac{k_z^*-k_0\beta_z}{k_{zz}^*+k_0\beta_x}\frac{k_x-k_0\beta_x}{k_x+k_0\beta_x}\times\frac{\exp\{ik_x(x+x_s)+ik_y y+ik_z^*(z+z_s)\}}{2k_z^*}dk_x\,dk_y. \tag{A10}$$

A convenient way to evaluate the integral is to use a spherical polar coordinate (R,μ,ε) centered at the image source, S_4. The receiver is located at (R_4,θ,ψ). Making use of the substitution: $k_x=k\cos\varepsilon\sin\mu$, $k_y=k\sin\varepsilon\sin\mu$, $k_z^*=k\cos\mu$ and $dk_x\,dk_y/k_z=k\sin\mu\,d\theta\,d\varepsilon$, we can transform Eq. (A10) to

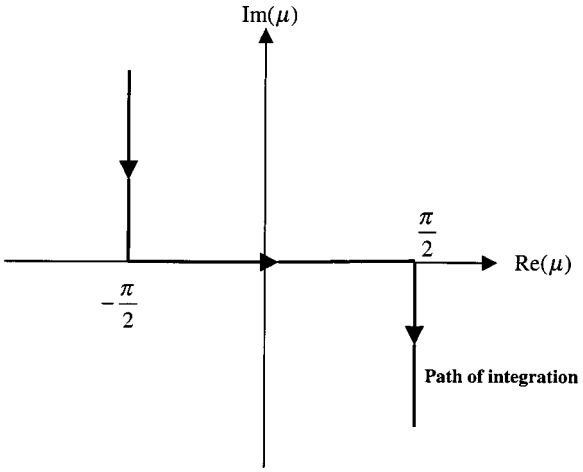

FIG. A1. The path of integration for the integral (A12).

$$I_4=\frac{-i}{2(2\pi)^2}\int_0^{\pi/2-i\infty}\int_0^{2\pi}\frac{\cos\mu-\beta_z}{\cos\mu+\beta_z}\frac{\cos\varepsilon\sin\mu-\beta_x}{\cos\varepsilon\sin\mu+\beta_x}\times e^{ikR_4\cos\theta\cos\mu}e^{ikR_4\sin\theta\sin\mu\cos(\varepsilon-\psi)}\sin\mu\,d\mu\,d\varepsilon. \tag{A11}$$

The integration with respect to ε can be evaluated by the method of stationary phase to give

$$I_4\approx\frac{ik}{4\pi}\int_{-\pi/2+i\infty}^{\pi/2-i\infty}\frac{\cos\mu-\beta_z}{\cos\mu+\beta_z}\frac{\cos\psi\sin\mu-\beta_x}{\cos\psi\sin\mu+\beta_x}\times H_0^{(1)}(kR_4\sin\theta\sin\mu)e^{ikR_4\cos\mu\cos\theta}\sin\mu\,d\mu, \tag{A12}$$

where $H_0^{(1)}(\ )$ is the Hankel function of the first kind. In obtaining Eq. (A12), the following identities[28] have been used:

$$H_0^{(1)}(z)\approx\sqrt{2/(i\pi z)}e^{iz},\quad H_0^{(2)}(z)\approx\sqrt{2i/(\pi z)}e^{-iz},$$

and

$$H_0^{(2)}(-z)=-H_0^{(1)}(z).$$

The path of integration for I_4 is shown in Fig. A1.

In addition to the required condition of θ_c close to $\pi/2$, we further restrict attention to the consideration of the situation where either the source or receiver is close to the façade. In this case, we have $\cos\psi\sin\theta_c\to1$. Hence, the only contribution due to the pole in the integrand of Eq. (A12) comes from the first quotient. We can use the method as detailed in Ref. 8 to evaluate the integral asymptotically. The approximate solution is

$$I_4\approx\frac{1}{4\pi}\frac{\cos\psi\sin\theta_c-\beta_x}{\cos\psi\sin\theta_c+\beta_x}Q(R_4,\theta_c,\beta_z)e^{ikR_4}. \tag{A13}$$

In the second case of interest, we have a small θ_c. We can use the same analysis as before to obtain the following asymptotic solution for I_4:

$$I_4\approx\frac{1}{4\pi}\frac{\cos\theta_c-\beta_z}{\cos\theta_c+\beta_z}Q(R_4,\Theta,\beta_z)e^{ikR_4}, \tag{A14}$$

where $\cos\Theta=\cos\psi\sin\theta_c$. To have a symmetric form for this reflected wave for multiple reflections from the ground and façade, we can include either a ''façade'' wave term in Eq. (A13) or a ground wave term in Eq. (A14). This leads to an interpretable expression

$$I_4\approx\frac{1}{4\pi}Q(R_4,\theta_c,\beta_x)Q(R_4,\Theta,\beta_z)e^{ikR_4}. \tag{A15}$$

[1] K. Heutshi, ''A simple method to evaluate the increase of traffic noise emission level due to buildings, for a long straight street,'' Appl. Acoust. **44**, 259–274 (1995).
[2] E. Wetzel, J. Nicolas, Ph. Andre, and J.-J. Boreux, ''Modeling the propagation pathway of street-traffic noise: Practical comparison of German guidelines and real-world measurements,'' Appl. Acoust. **57**, 97–107 (1999).
[3] E. Walerian, R. Janczur, and M. Czechowicz, ''Sound level forecasting for city centers. I: Sound level due to a road within an urban canyon,'' Appl. Acoust. **62**, 359–380 (2001).
[4] *Calculation of Road Traffic Noise* (H. M. Stationery Office, London, 1988).
[5] E. Walerian and R. Janczur, ''Effect of source model parameters on sound level in built-up area,'' Arch. Acoust. **24**, 145–160 (1999).
[6] J. Nicolas, J. L. Berry, and G. A. Daigle, ''Propagation of sound above a finite layer of snow,'' J. Acoust. Soc. Am. **77**, 67–73 (1985).
[7] K. K. Iu and K. M. Li, ''The propagation of sound in city streets,'' Proceedings of Westprac VII, Vol. 2, 811–814, Kumamoto, Japan (2000).
[8] C. F. Chien and W. W. Soroka, ''A note on the calculation of sound propagation along an impedance plane,'' J. Sound Vib. **69**, 340–343 (1980).
[9] S. N. Chandler-Wilde, ''Ground effects in environmental sound propagation,'' Ph.D. thesis, University of Bradford, 1988.
[10] T. F. W. Embleton, ''Tutorial on sound propagation outdoors,'' J. Acoust. Soc. Am. **100**, 31–48 (1996).
[11] A. D. Pierce, *Acoustics: An Introduction to its Physical Principles and Applications* (Acoustical Society of America, New York, 1989).
[12] K. Attenborough, ''Review of Ground effects on outdoor sound propagation from continuous broadband sources,'' Appl. Acoust. **24**, 289–319 (1988).
[13] T. Kawai, T. Hidaka, and T. Nakajima, ''Sound propagation above an impedance boundary,'' J. Sound Vib. **83**, 125–138 (1982).
[14] S. I. Thomasson, ''Reflection of waves from a point source by an impedance boundary,'' J. Acoust. Soc. Am. **59**, 780–785 (1976).
[15] K. Attenborough, S. Taherzadeh, H. E. Bass, X. Di, R. Raspet, G. R. Becker, A. Güdesen, A. Chrestman, G. A. Daigle, A. L'Espérance, Y. Gabillet, K. E. Gilbert, Y. L. Li, M. J. White, P. Naz, J. M. Noble, and H. A. J. M. van Hoof, ''Benchmark cases for outdoor sound propagation models,'' J. Acoust. Soc. Am. **97**, 173–191 (1995).
[16] L. R Quartararo, ''A theoretical investigation of sound propagation above a half-space of extended reaction,,'' MS thesis, Penn. State University, March, 1993.
[17] K. Attenborough, N. W. Heap, T. L. Richards, and V. V. S. S. Sastry, ''Comments on ground effect analysis: Surface wave and layer potential representation,'' J. Sound Vib. **84**, 289–295 (1982).
[18] C. H. Howorth, ''Sound propagation over rigid porous layers,'' Ph.D. thesis, The Open University, 1991.
[19] K. Attenborough, ''Ground parameter information for propagation modeling,'' J. Acoust. Soc. Am. **92**, 418–427 (1992).
[20] M. E. Delany and E. N. Bazley, ''Acoustical properties of fibrous absorbent materials,'' Appl. Acoust. **3**, 105–116 (1970).
[21] K. M. Li, T. Waters-Fuller, and K. Attenborough, ''Sound propagation from a point source over extended-reaction ground,'' J. Acoust. Soc. Am. **104**, 679–685 (1998).
[22] D. D. Rife, ''Maximum-Length Sequence System Analyzer, Reference Manual,'' Version 10W, 1987–1988.
[23] K. V. Horoshenkov, D. C. Hothersall, and S. E. Mercy, ''Scale modeling of sound propagation in a city street canyon,'' J. Sound Vib. **223**, 795–819 (1999).
[24] US Department of Transportation, *FHWA Traffic Noise Model, Technical Model* (Federal Highway Administration, Office of Environment and Planning, Washington, D.C.).
[25] J. Lighthill, ''Asymptotic behaviour of anisotropic wave systems stimulated by oscillated sources,'' in *Wave Asymptotics*, edited by P. A. Martin and G. R. Wickham (Cambridge University Press, Cambridge, 1992),

Chap. 1. See also J. Lighthill, ''Emendations to a proof in the general three-dimensional theory of oscillating sources of waves,'' Proc. R. Soc. London, Ser. A **427**, 31–42 (1990).
[26] L. M. Brekhovskikh, *Waves in Layered Media* (Academic, New York, 1980), p. 228.
[27] C. F. Chien and W. W. Soroka, ''Sound propagation along an impedance plane,'' J. Sound Vib. **43**, 9–20 (1975).
[28] M. Abramowitz and I. A. Stegun, *Handbook of Mathematical Functions with Formulas, Graphs, and Mathematical Tables* (Dover, New York, 1972).